Supplementary Information

Ultrathin MoS_2 Flakes Embedded in Nanoporous Graphene Films for a Multi-Functional Electrode

Sung-Wook Kim, Jongha Hwang, Seong-Ji Ha Jae-Eun Lee, Jong-Chul Yoon and Ji-Hyun Jang *

[1]School of Energy and Chemical Engineering, Ulsan National Institute of Science and Technology, Ulsan 689-798, Republic of Korea

……

*Corresponding author: Fax: 82-52-217-3008; Tel: 82-52-217-2922

Email: clau@unist.ac.kr (Ji-Hyun Jang)

Calculation of capacitance of supercapacitors

The volumetric specific capacitance (C_a, F cm^{-3}) was determined based on the GDC curves using the following equation:

$$C_{cell} = I/(\Delta V/\Delta t) \quad (1)$$

Where ΔV, I, and Δt correspond to the potential window (excluding IR drop), discharge time and discharge current, respectively. The volumetric capacitance (C_v) of the mSC was calculated according to the equation, $C_v = C_{cell}/V_{cell}$, where V_{cell} is the total effective volume of the mSC is determined by the active volume of micro-supercapacitor (0.0001071 cm^3, see Figure S10), the summation of both positive and negative electrode area. (The areal capacitance of MoS2/NGF is 9.9 mF cm^{-2})

The energy density (E) and power density (P) of the device were calculated based on the following equations:

$$E = 1/2 C_v \Delta V^2 \quad (2)$$

$$P = E/\Delta t \quad (3)$$

$$E = \frac{1}{2 \times 3600} \times 55 F/cm^3 \times 1^2 = 0.00763\ Wh/cm^3$$

$$P = \frac{0.00763\ Wh/cm^3}{28s} \times 3600 = 1\ Wh/cm^3$$

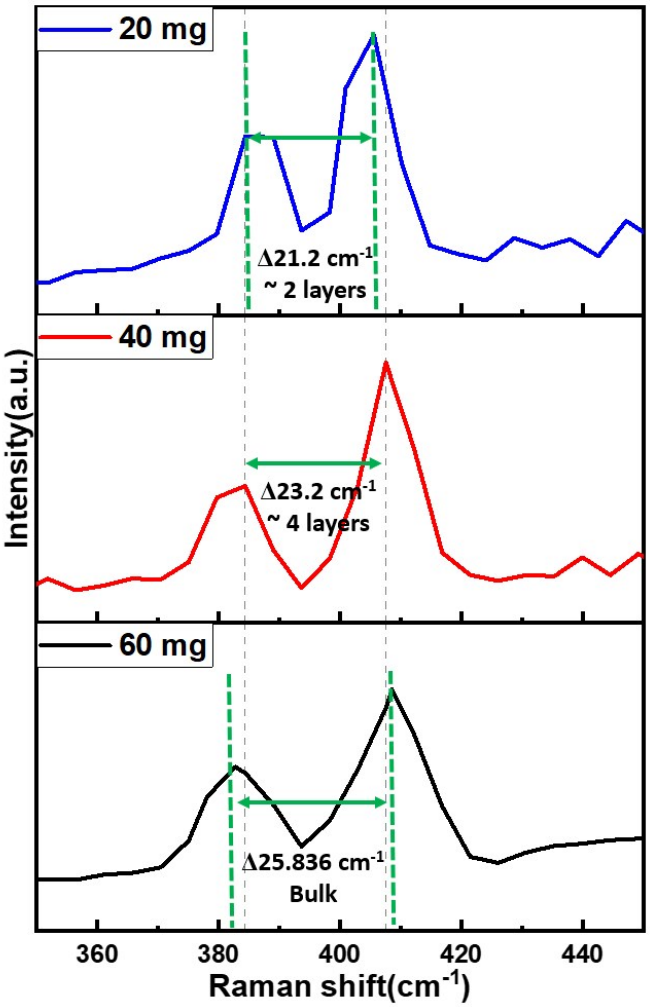

Figure S1. Raman spectra of 2H-MoS_2 with different concentration of ATTM.

The optimized content of ammonium tetrathiomolybdate (ATTM, 40 mg) to create few-layer MoS_2 sheets was determined by the Raman spectra. A 20 mg sample was discarded due to low yield.

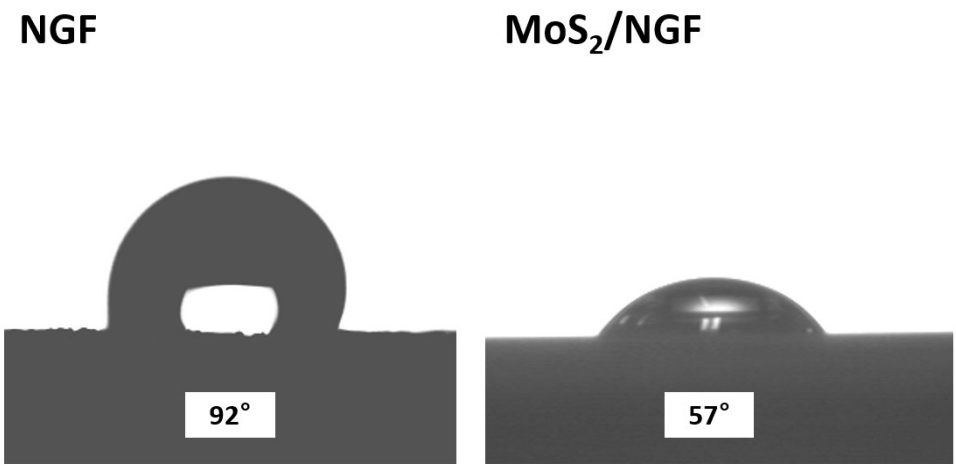

Figure S2. Contact angle of NGF and MoS_2/NGF.

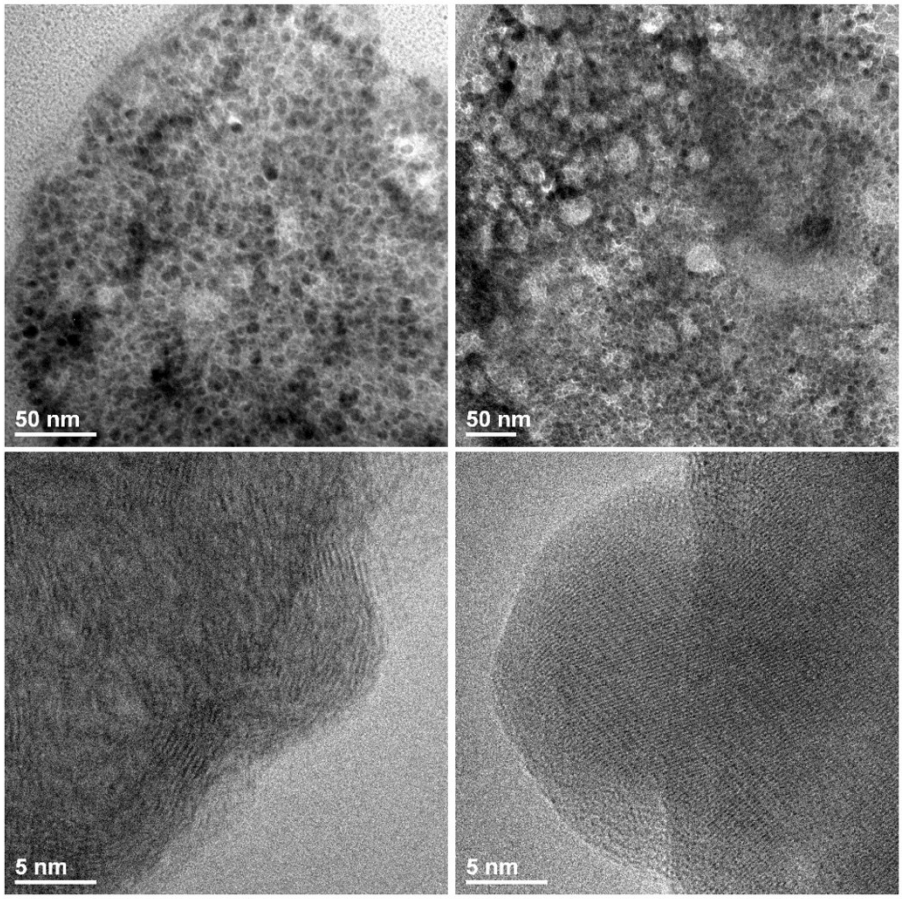

Figure S3. Low-magnification TEM images of MoS_2/NGF.

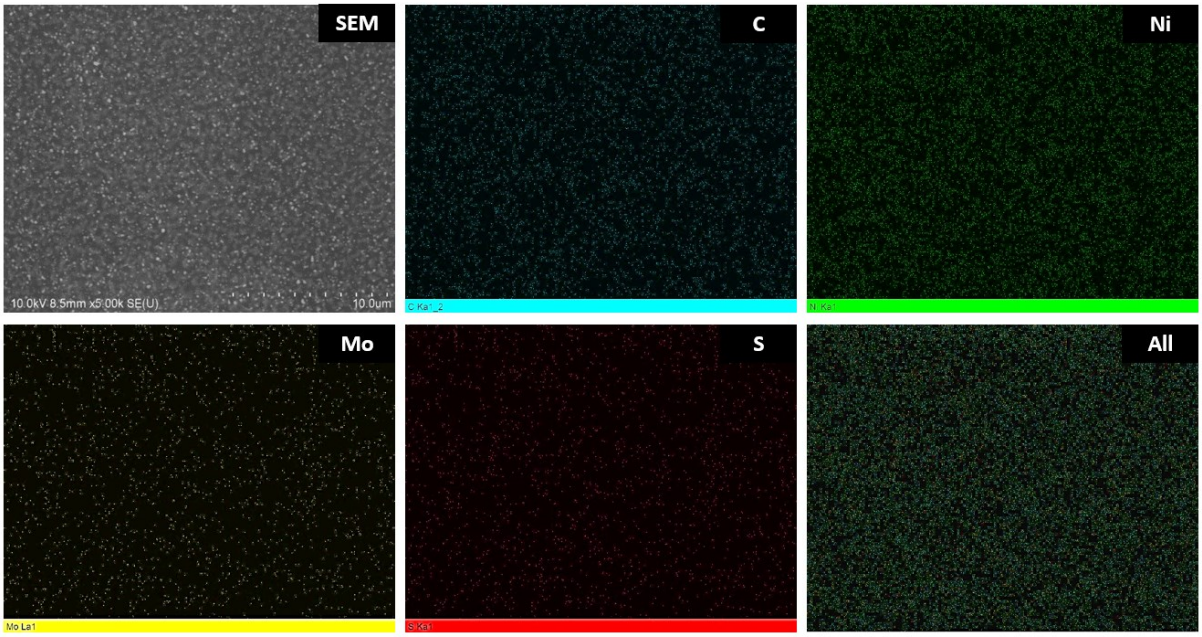

Figure S4. EDAX mapping of the elements present in MoS_2/NGF.

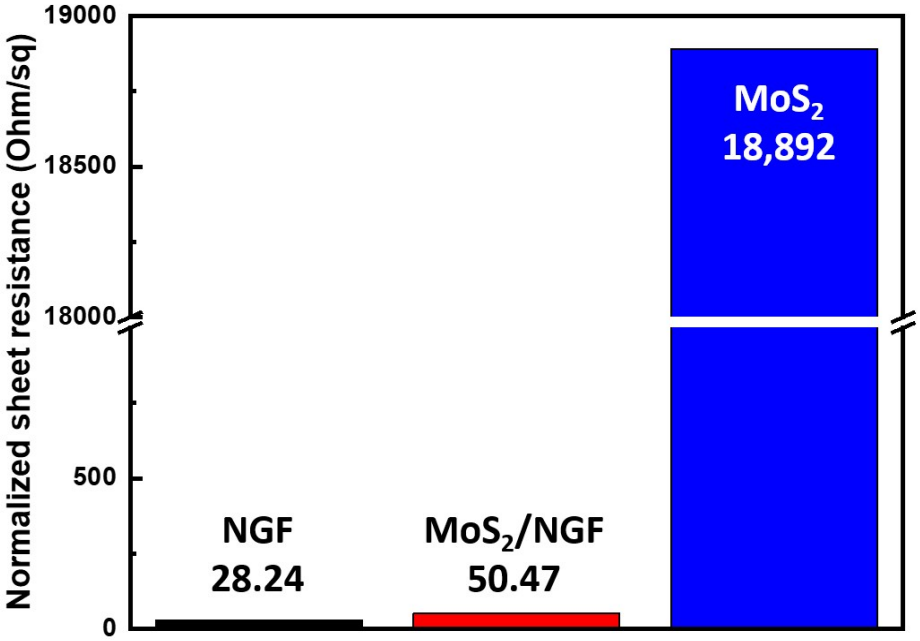

Figure S5. Normalized sheet resistance of NGF, MoS_2/NGF and MoS_2.

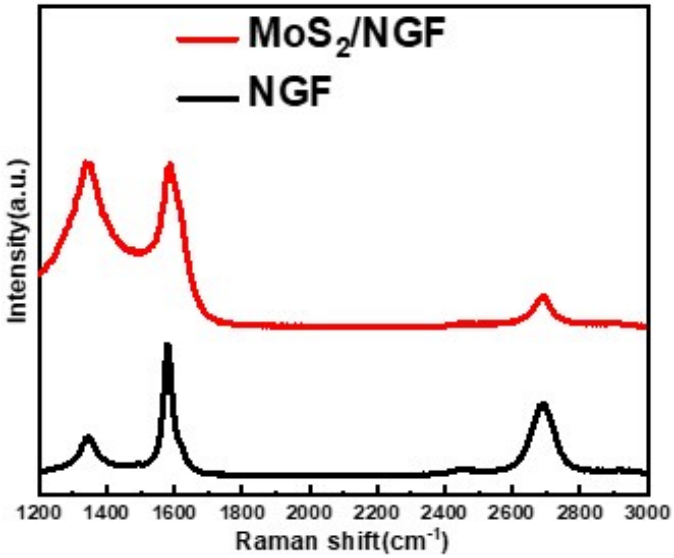

Figure S6. Raman spectra of NGF and MoS_2/NGF.

NGF displayed a D peak at around 1347 cm^{-1}, a sharp G peak at 1588 cm^{-1}, and a 2D peak at 2697 cm^{-1}. Compared to pristine NGF, MoS_2/NGF exhibited a much higher intensity in the D peak, suggesting that the ultrathin MoS_2 promotes the formation of defect sites for hydrogen-sulfide binding.

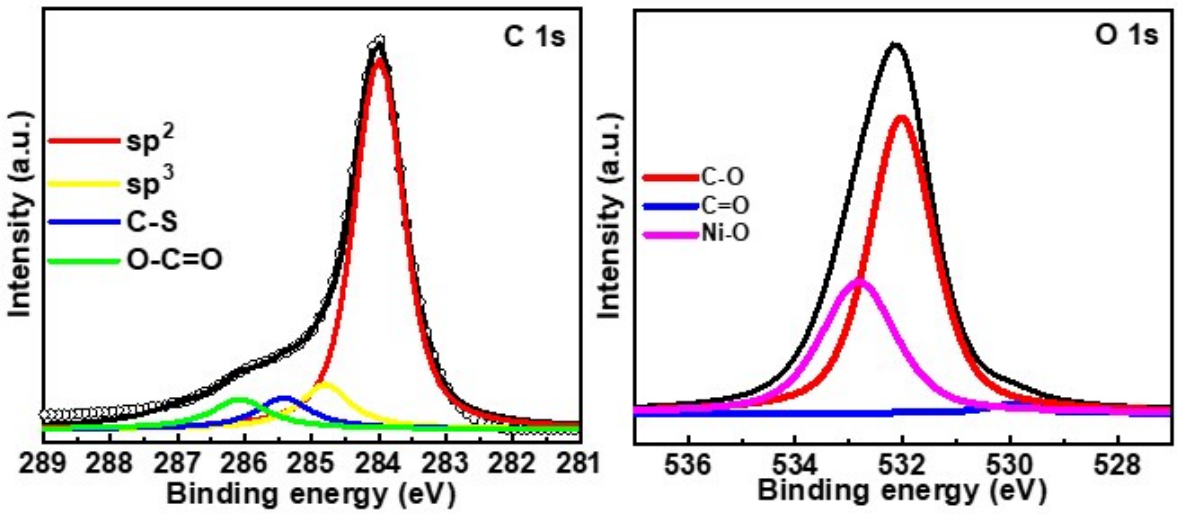

Figure S7. X-ray photo-electron spectroscopy (XPS) of the MoS_2/NGF: c) C1s, d) O1s

Figure S7 shows the XPS C 1s spectrum of MoS_2/NGF. C 1s peaks of the as-prepared MoS_2/NGF were deconvoluted into four peaks at binding energies of 284.0 (sp^2 carbon peak), 284.8 (sp^3), 285.3 (covalent C-S), 286.1 (C-O) eV, which suggested the presence of functional groups at edge sites and defects in the inner pores. The result of O 1s spectra indicated the presence of different oxygen functional groups, such as C-O, C=O and Ni-O at binding energies of 532.0 eV, 529.2 eV and 532.8 eV, respectively.

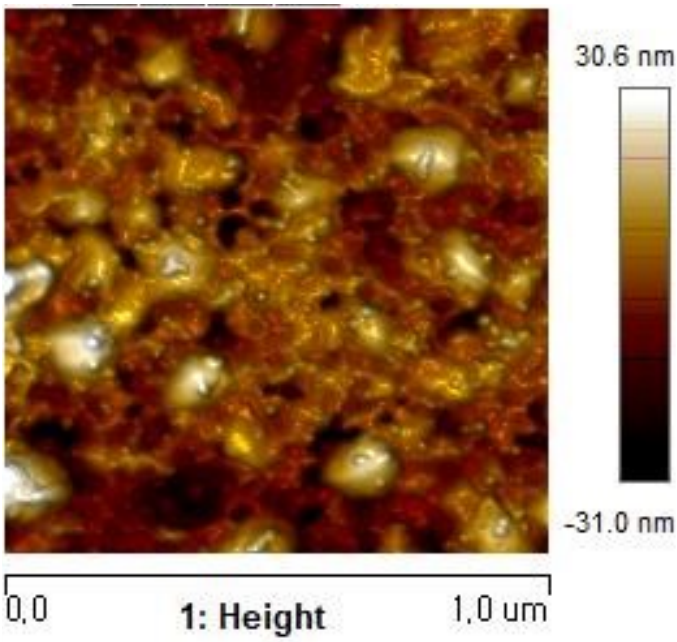

Figure S8. Atomic force microscopy image of MoS_2/NGF film.

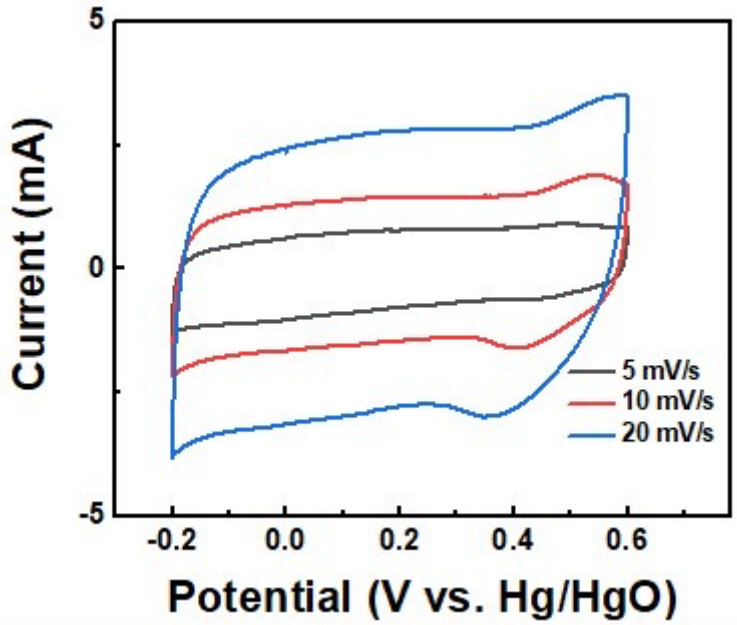

Figure S9. Cyclic voltammogram profiles of MoS_2/NGF in the three-electrode system.

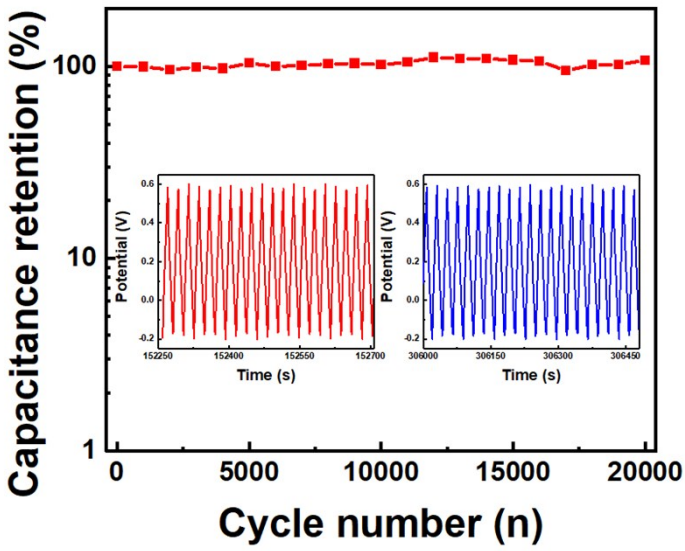

Figure S10. Capacitance retention of MoS_2/NGF in the three-electrode system.

We achieved almost 100 % of capacitance retention after 20,000 cycles in 1M sulfuric acid electrolyte in the three-electrode system.

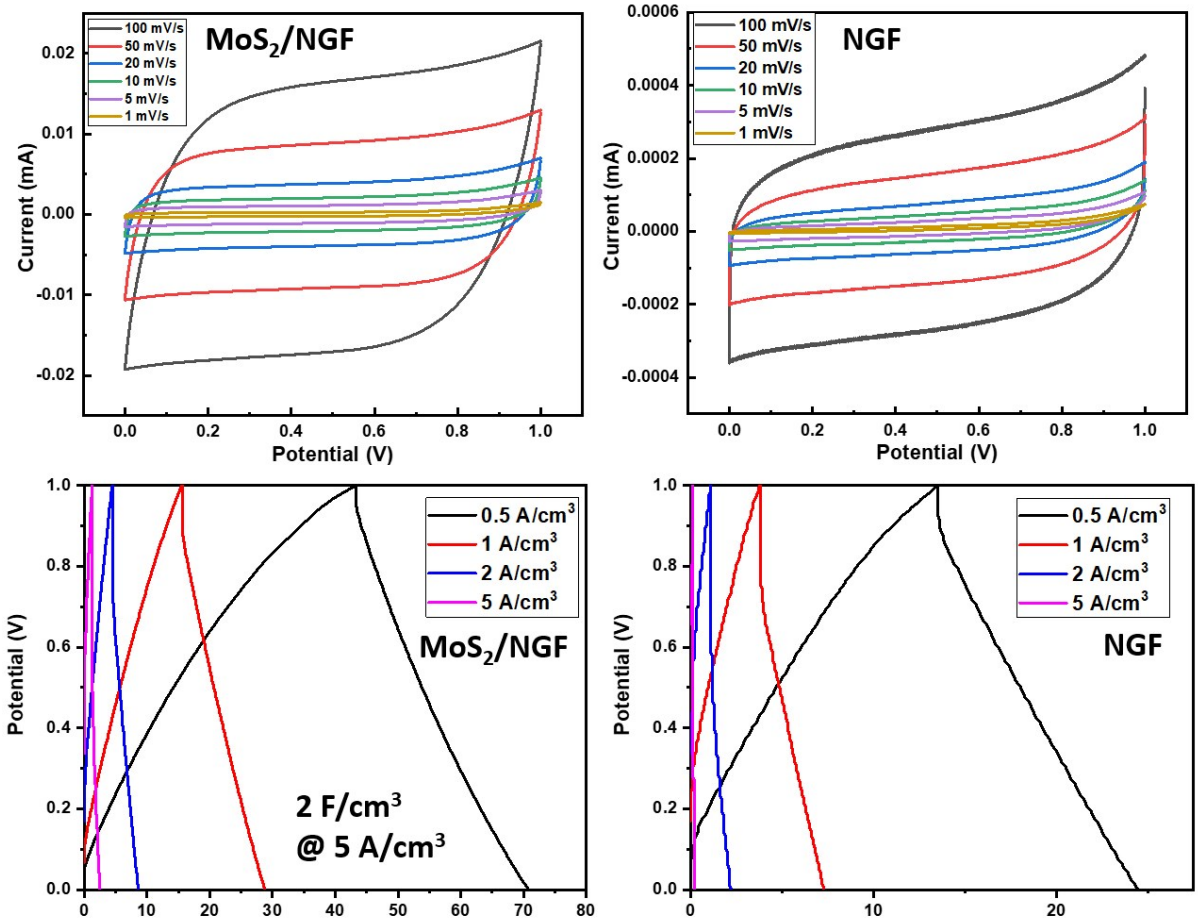

Figure S11. Cyclic voltammogram profiles of the NGF and MoS_2/NGF mSC (scan rate = 1 to 100 mV s^{-1}) and galvanostatic charge/discharge curves of the NGF and MoS_2/NGF mSC.

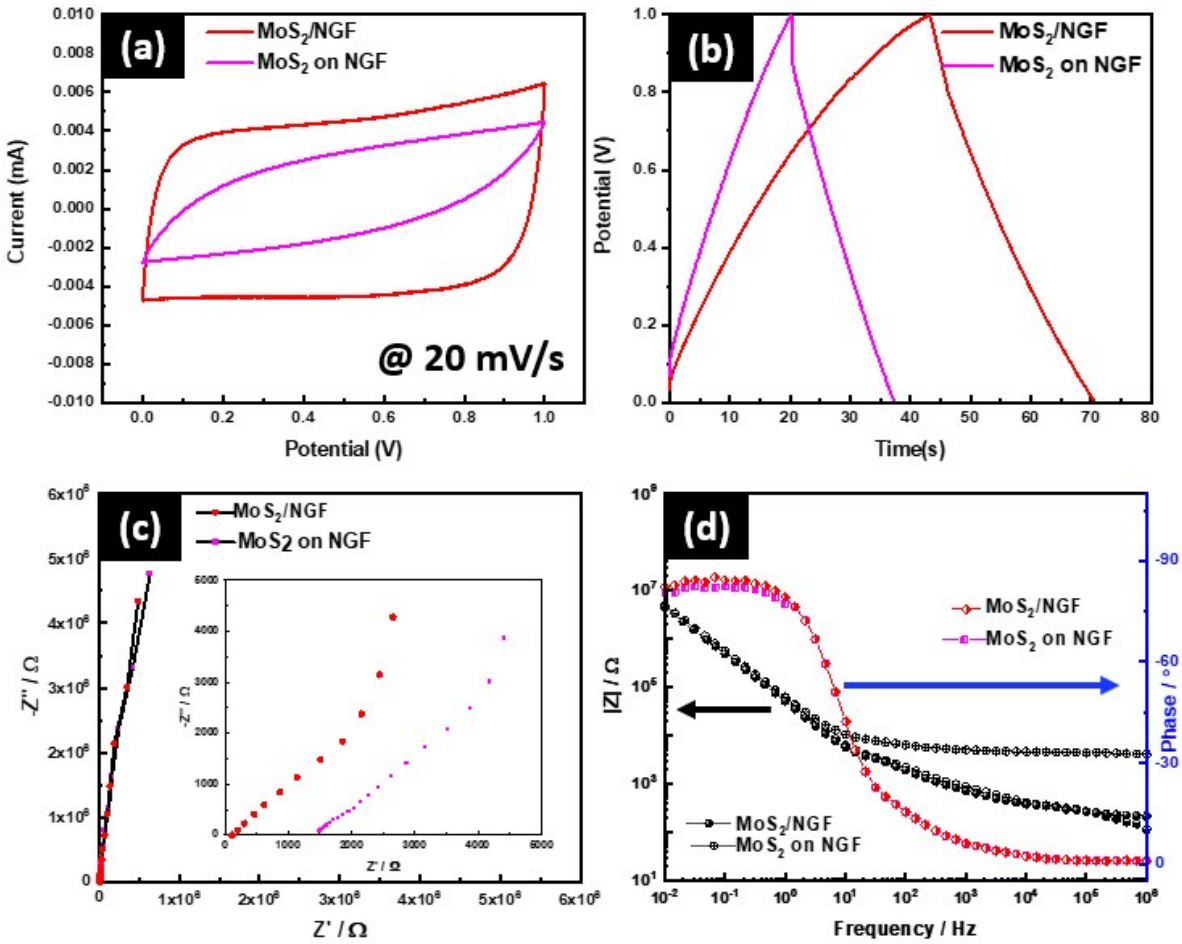

Figure S12. (a) Cyclic voltammogram profiles of the MoS_2 on NGF (simple deposition) and MoS_2/NGF (direct growth) mSC (scan rate = 20 mV s^{-1}). b) Galvanostatic charge/discharge curves of the MoS_2 on NGF and MoS_2/NGF mSC (current density = 1 A cm^{-3}). c) Nyquist plot of the MoS_2 on NGF and MoS_2/NGF mSC. The inset is a close-up image at the high frequency region. d) Bode plot of the MoS_2 on NGF and MoS_2/NGF mSC.

Figure **S12a** shows the CV curves of a single unit mSC in the potential window of 0-1.0V. MoS_2/NGF showed a rectangular shape than simple MoS_2 loading on NGF, indicating the improved capacitive performances originated from the interconnected structure of MoS_2/NGF. Figure **S12b** shows the galvanostatic charge/discharge curves (GCD) at a current density of 0.5 A cm^{-3}. MoS_2/NGF and MoS_2 on NGF retained a quasi-triangular shape, but MoS_2 on NGF shows much higher IR drop during discharge process. Figure **S12c**, The MoS_2/NGF mSC exhibited a smaller equivalent circuit resistance (215 Ω) compared to MoS_2 on NGF (1,500 Ω). The phase angle of the mSC was almost same for the MoS_2/NGF and MoS_2 on NGF.

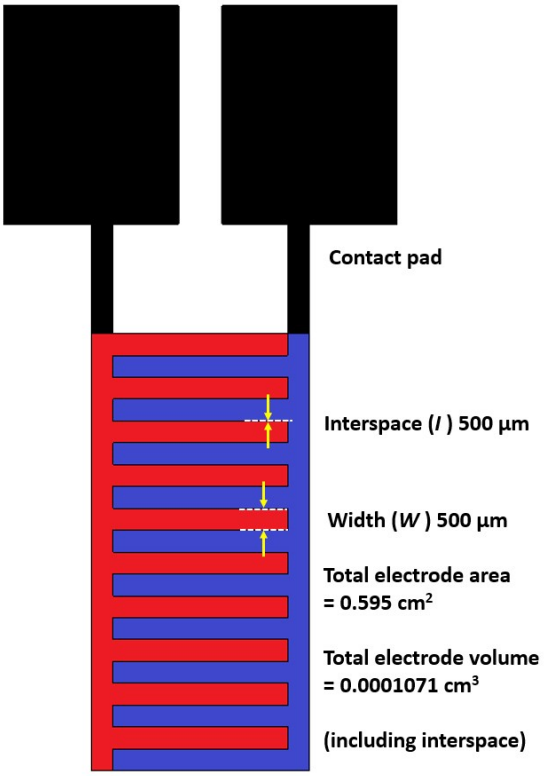

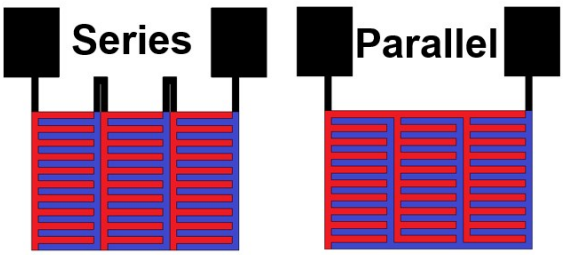

Total electrode area = 1.785 cm²
Total electrode volume = 0.0003213 cm³

Material	Thickness
PET layer	20 μm
MoS_2/NFG layer	1.8 μm

Figure S13. Dimensional information of single, series and parallel integrated MoS_2/NGF micro-supercapacitor and cross-sectional schematic image of micro-supercapacitor

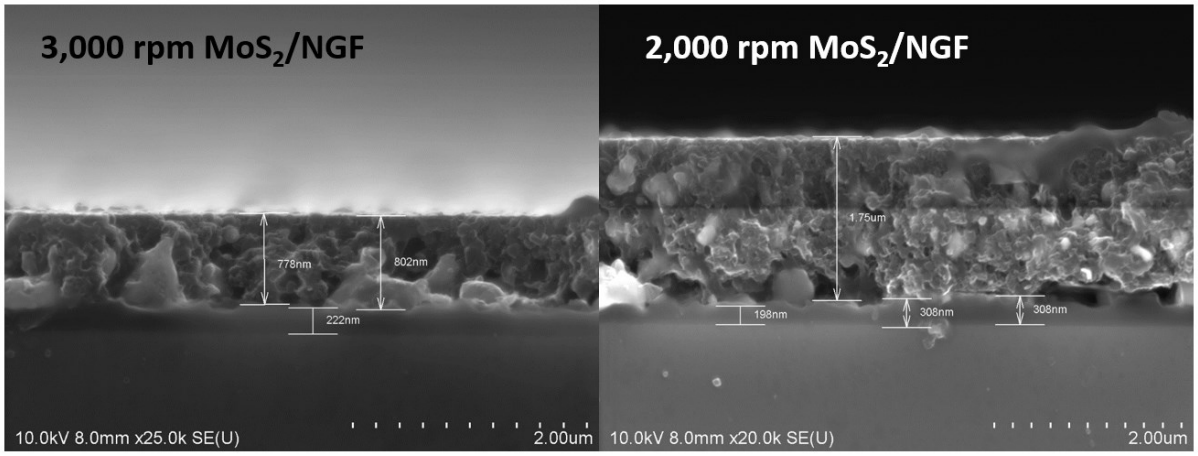

Figure S14. Cross-sectional SEM images of MoS_2/NGF film.

The thicknesses of MoS_2/NGF, controlled by adjusting the spin-coating rate, were 800 nm and 1.8 μm for 3,000 rpm and 2,000 rpm, respectively.

Table S1. Comparison of micro-supercapacitors.

Active Material	Method	Current Collector	Potential Window	Electrolyte	Specific Capacitance	Ref. No.
Co_3O_4	Lithography /Sputtering deposition	Cr	2V	LiPON	14 F/cm^3 @ RT 37 F/cm^3 @ 90 C°	8
MoS_2-LIG	CO_2 Laser beam	MoS_2-LIG	1V	PVP/NaCl	16mF/cm^2	9
MnO_x	Electron beam evaporation	Au/Cr	0.8 V	PVA/H_2SO_4	32.8 F/cm^3	10
MWCNT	Plasma jet etching	MWCNT	0.8 V	PVA/H_3PO_4	2.02 F/cm^3	15
rGO	Pulsed UV laser	rGO	1.2 V	0.1M Na_2SO_4	288.7 mF/cm^3	11
GO ink	3D Printing	Au	1V	PVA/H_2SO_4	828.06 mF/cm^3	12
$Cu(OH)_2$@ FeOOH nanotube	Screen printing	Cu	1.5 V	Fumed silica [EMIM][BF_4] ionogel	32.2 F/cm^3	32
MWCNT /Mn_3O_4	Photolithography LBL assembly	E-beam Ti/Au	1.2 V	PMMA-PC-$LiClO_4$	8.9 F/cm^3	S8
Photoresist derived porous carbon	Photolithography	Cu/Ni tape	0.8 V	0.5 M H_2SO_4	11 F/cm^3	24
MoS_2/NGF	Film transfer	NGF	1 V	PVA/H_3PO_4	55 F/cm^3	This work

Table S2. Comparison of energy/power densities of micro-supercapacitors.

Active Material	Max energy density	Max power density	Ref. No.
Carbon	0.18 mWh cm^{-3}	0.4 W cm^{-3}	15
LbL-MWNT/Mn_3O_4	1.8 mWh cm^{-3}	4.4 W cm^{-3}	S8
PEDOT	2.98 mWh cm^{-3}	0.42 W cm^{-3}	25
C/CHIT-CNT	4.5 mWh cm^{-3}	0.20 W cm^{-3}	26
MWNT/Mn_3O_4	2.4 mWh cm^{-3}	8 W cm^{-3}	S12
LSG/ZnO	1.2 mWh cm^{-3}	0.07 W cm^{-3}	27
GO	0.43 mWh cm^{-3}	9.4 W cm^{-3}	28
$Bi_6O_6(OH)_3](NO_3)_3$• $1.5H_2O$ $Bi_2O(OH)_2SO_4$	0.125 mWh cm^{-3}	0.053 W cm^{-3}	33
3D printing CNT	0.12 mWh cm^{-3}	3.72 W cm^{-3}.	19
MoS_2/NGF	7.64 mWh cm^{-3}	9.96 W cm^{-3}	This work

Table S3. Specific capacitance changes according to the electrode thickness of MoS_2/NGF.

Thickness by rpm	Capacitance
2.5 μm 1,000 rpm	80 F/cm^3 (Brittle)
1.8 μm 2,000 rpm	55 F/cm^3 (Flexible)
800 nm 3,000 rpm	13 F/cm^3 (Flexible)

References

[1] T. Göhlert, P. F. Siles, T. Päßler, R. Sommer, S. Baunack, S. Oswald, O. G. Schmidt, *Nano Energy* **2017**, *33*, 387.

[2] F. Clerici, M. Fontana, S. Bianco, M. Serrapede, F. Perrucci, S. Ferrero, E. Tresso, A. Lamberti, *ACS Appl Mater Interfaces* **2016**, *8*, 10459.

[3] W. Si, C. Yan, Y. Chen, S. Oswald, L. Han, O. G. Schmidt, *Energy & Environmental Science* **2013**, *6*.

[4] L. Liu, D. Ye, Y. Yu, L. Liu, Y. Wu, *Carbon* **2017**, *111*, 121.

[5] R. Kumar, R. Savu, E. Joanni, A. R. Vaz, M. A. Canesqui, R. K. Singh, R. A. Timm, L. T. Kubota, S. A. Moshkalev, *RSC Advances* **2016**, *6*, 84769.

[6] W. Li, Y. Li, M. Su, B. An, J. Liu, D. Su, L. Li, F. Li, Y. Song, *Journal of Materials Chemistry A* **2017**, *5*, 16281.

[7] J.-Q. Xie, Y.-Q. Ji, J.-H. Kang, J.-L. Sheng, D.-S. Mao, X.-Z. Fu, R. Sun, C.-P. Wong, *Energy & Environmental Science* **2019**, *12*, 194.

[8] G. Lee, D. Kim, D. Kim, S. Oh, J. Yun, J. Kim, S.-S. Lee, J. S. Ha, *Energy & Environmental Science* **2015**, *8*, 1764.

[9] M. S. Kim, B. Hsia, C. Carraro, R. Maboudian, *Carbon* **2014**, *74*, 163.

[10] A. Liu, P. Kovacik, N. Peard, W. Tian, H. Goktas, J. Lau, B. Dunn, K. K. Gleason, *Adv Mater* **2017**, *29*.

[11] Y. Yang, L. He, C. Tang, P. Hu, X. Hong, M. Yan, Y. Dong, X. Tian, Q. Wei, L. Mai, *Nano Research* **2016**, *9*, 2510.

[12] S. Y. Hong, J. Yoon, S. W. Jin, Y. Lim, S. J. Lee, G. Zi, J. S. Ha, *ACS Nano* **2014**, *8*, 8844.

[13] M. H. Amiri, N. Namdar, A. Mashayekhi, F. Ghasemi, Z. Sanaee, S. Mohajerzadeh, *Journal of Nanoparticle Research* **2016**, *18*.

[14] W. Gao, N. Singh, L. Song, Z. Liu, A. L. Reddy, L. Ci, R. Vajtai, Q. Zhang, B. Wei, P. M. Ajayan, *Nat Nanotechnol* **2011**, *6*, 496.

[15] Z. Liu, F. Teng, C. Chang, Y. Teng, S. Wang, W. Gu, Y. Fan, W. Yao, Y. Zhu, *Nano Energy* **2016**, *27*, 58.

[16] W. Yu, H. Zhou, B. Q. Li, S. Ding, *ACS Appl Mater Interfaces* **2017**, *9*, 4597.